The Impact of Ocean Surface Currents on Sverdrup Transport in the Midlatitude North Pacific via the Wind Stress Formulation

ZHITAO YU, E. JOSEPH METZGER, AND YALIN FAN

Naval Research Laboratory, Stennis Space Center, Mississippi

(Manuscript received 1 July 2016, in final form 20 December 2016)

ABSTRACT

A more complete wind stress $\boldsymbol{\tau}_n$ formulation takes into account the ocean surface currents $\mathbf{V}_o$, while the conventional wind stress $\boldsymbol{\tau}_c$ popularly used in ocean circulation models is only a function of 10-m winds $\mathbf{V}_{10}$. An analytical solution is derived for the difference of Sverdrup transport induced by using $\boldsymbol{\tau}_n$ instead of $\boldsymbol{\tau}_c$. A scaling analysis of the analytical solution indicates a 6% reduction of the Sverdrup transport in the North Pacific (i.e., the Kuroshio transport in the East China Sea) when Ekman velocity dominates the ocean surface currents. Because of the quadratic nature of wind stress, four nonlinear terms contribute equally to this difference: two vorticity torque terms and two speed gradient torque terms. A pair of 12.5-yr (July 2002–14) Hybrid Coordinate Ocean Model simulations that only differ in the wind stress formulation are used to test the analytical solution. The model results (2004–14) confirm that using $\boldsymbol{\tau}_n$ instead of $\boldsymbol{\tau}_c$ reduces the Sverdrup transport in the North Pacific by 8%–17% between 23° and 32°N. The reduction rate of the simulated 11-yr mean Kuroshio transport through the East Taiwan Channel and Tokara Strait is 8.0% (−2.5 Sv; 1 Sv $\equiv 10^6$ m^3 s^{-1}) and 12.8% (−4.8 Sv), respectively, in good agreement with the Sverdrup transport reduction rate, which is 7.4% (−2.6 Sv) and 15.4% (−6.3 Sv) at the corresponding latitude. The local effect of changing wind stress/wind work and Ekman transport due to the inclusion of $\mathbf{V}_o$ in the wind stress formulation is negligible compared to the Kuroshio volume transport change estimated in this study.

1. Introduction

The Sverdrup transport serves as a cornerstone of the wind-driven, large-scale ocean circulation theory (Wunsch and Roemmich 1985). It is a steady-state solution and in the form of $M = (\nabla \times \boldsymbol{\tau})/\beta$, where M is the mass Sverdrup transport, $\boldsymbol{\tau}$ is the surface wind stress, and β is the variation of Coriolis parameter f with latitude (Sverdrup 1947). Thus, accurate calculation of the surface wind stress is essential for the large-scale ocean circulation.

Conventionally, surface wind stress $\boldsymbol{\tau}_c$ (the subscript c stands for conventional) is calculated using the bulk algorithm as

$$\boldsymbol{\tau}_c = \rho_{\text{air}} C_d |\mathbf{V}_{10}| \mathbf{V}_{10}, \tag{1}$$

where ρ_{air} is the air density at sea level, C_d is the drag coefficient, and $\mathbf{V}_{10}$ is the 10-m wind velocity relative to the solid earth (Pacanowski 1987). When we apply this formula over the ocean, it is the relative motion at the air–sea interface that produces the wind stress. Thus, the shear velocity between 10-m winds and the ocean surface currents should be used. A more complete wind stress formulation $\boldsymbol{\tau}_n$ (the subscript n stands for new method) that includes the underlying ocean is

$$\boldsymbol{\tau}_n = \rho_{\text{air}} C_d |\mathbf{V}_{10} - \mathbf{V}_o| (\mathbf{V}_{10} - \mathbf{V}_o), \tag{2}$$

where $\mathbf{V}_o$ is the velocity of ocean surface currents that is typically much smaller than $\mathbf{V}_{10}$ and thus does not significantly change the wind stress magnitude. Therefore, the conventional wind stress formulation [Eq. (1)] is still commonly used (Duhaut and Straub 2006) in ocean general circulation models.

However, the importance of strong ocean surface currents in modifying the wind stress has been demonstrated by several observational studies. Cornillon and Park (2001) find a clear signature of Gulf Stream warm-core rings in the NASA Scatterometer (NSCAT) data. The Gulf Stream and Kuroshio are also apparent in the 4-yr average of the wind stress curl calculated using the Quick Scatterometer (QuikSCAT) data (Chelton et al. 2004). Kelly et al. (2001) show that the difference

Naval Research Laboratory Contribution Number NRL/JA/7320-16-2895.

Corresponding author e-mail: Zhitao Yu, zhitao.yu@nrlssc.navy.mil

DOI: 10.1175/JPO-D-16-0155.1

between NSCAT wind speeds and those measured by Tropical Atmosphere Ocean anemometers can be explained by the surface currents measured by buoys in the South Equatorial Current region, and they find that the $\mathbf{V}_o$ dependence reduces the median wind stress magnitude by 20%. Analyzing QuikSCAT data and SSH fields from Collecte Localis Satellites/Archiving, Validation, and Interpretation of Satellite Oceanographic, Gaube et al. (2015) demonstrate that the eddy-induced Ekman pumping velocity arising from taking into account $\mathbf{V}_o$ approaches $O(10)$ cm day^{-1} on average and attenuates the eddies. Additionally, analysis of QuikSCAT data, satellite altimetry, and drifter data (Hughes and Wilson 2008; Xu and Scott 2008) suggest that wind work can be reduced by 20%–35% when $\mathbf{V}_o$ is included in the wind stress formulation.

Numerical studies indicate that including $\mathbf{V}_o$ in the wind stress formulation leads to improvements in ocean simulations in the tropical Atlantic Ocean (Pacanowski 1987) and the tropical Pacific Ocean (Luo et al. 2005). Dewar and Flierl (1987) suggest that the top drag induced by $\mathbf{V}_o$ can spin down Gulf Stream rings. Using an idealized 3-layer quasigeostrophic simulation, Duhaut and Straub (2006) find a 20%–35% reduction of wind work when $\mathbf{V}_o$ is included in the wind stress calculation. Dawe and Thompson (2006) drew a similar conclusion with a 27% reduction of wind work using numerical simulations with a 1/5° 20-layer isopycnal model. In addition, eddy-resolving 1/12.5° global Hybrid Coordinate Ocean Model (HYCOM) simulations suggest that the total number of mesoscale eddies is reduced when ocean surface currents are included in the wind stress formulation (J. Shriver 2016, personal communication).

Numerical simulations further suggest that the reduction of wind work leads to the reduction of surface eddy kinetic energy (EKE). In a numerical study of the northwest Atlantic Ocean, Zhai and Greatbatch (2007) find that the $\mathbf{V}_o$ dependence of the wind stress formulation reduces the total wind work by 17% and the modeled EKE decreases by about 10% in response to direct mechanical damping by the surface wind stress. Model results in the tropical Atlantic Ocean (Eden and Dietze 2009) suggest a 50% EKE reduction when Eq. (2) is used, and the difference in wind work is the predominant driver for the reduction of EKE. Utilizing the Scripps Coupled Ocean–Atmosphere Regional Model (Weather Research and Forecasting Model coupled with Regional Ocean Modeling System) to study the California Current System, Seo et al. (2016) demonstrate that spatially averaged surface EKE is reduced by 44% primarily due to the enhanced surface eddy drag and reduced wind energy transfer when $\mathbf{V}_o$ is included in the wind stress formulation. Renault et al. (2016) further demonstrate that the EKE reduction is overestimated when not considering the feedback of ocean surface currents on the wind.

The preceding observational and numerical studies have demonstrated the important local effect of $\mathbf{V}_o$. However, none of them investigates the remote effect of $\mathbf{V}_o$ on western boundary currents, that is, on the return flow of Sverdrup transport in the ocean interior. Since taking into account the velocity shear across the air–sea interface ($\mathbf{V}_{10} - \mathbf{V}_o$) reduces the wind energy input and EKE as discussed above, it is natural to think this will weaken the mean energetics of the wind-driven circulation and thus mean volume transport. However, wind work is not the only energy source of the kinetic energy (KE) in the mean flow (Winters et al. 1995; Hughes et al. 2009); shear production of EKE from the mean shear and reversible buoyancy flux of the mean flow also contribute to the mean KE evolution. Thus, the change of mean KE (or transport) due to the $\mathbf{V}_o$ dependence is not trivial.

In this study, we examine the impact of wind stress formulation (with and without ocean surface currents) on Sverdrup transport through both analytical solutions and numerical simulations using global HYCOM with 1/12.5° resolution. The numerical results are further used to analyze the effect of the wind stress formulation on the Kuroshio transport entering and exiting the East China Sea (ECS), and its relationship with the Sverdrup transport in the midlatitude North Pacific Ocean. The coherent wind response to mesoscale sea surface temperature (SST) has been broadly observed in the global ocean (Park and Cornillon 2002; Xie 2004; Chelton and Xie 2010; O'Neill et al. 2010, 2012; Frenger et al. 2013). Previous studies also suggest that wind curl is correlated to the SST gradient (Chelton et al. 2001, 2004). This effect is not the focus of the current study, in which the wind stress is not allowed to vary with SST directly but only through C_d.

This paper is organized as follows: Sections 2 describes the numerical model and experimental configuration. An analytical solution of the Sverdrup transport difference is derived in section 3. Model results are presented and analyzed in section 4, which is followed by discussion and conclusions in section 5.

2. Numerical simulations

HYCOM is widely used in the ocean community (http://www.hycom.org) and is the ocean model component for the present operational U.S. Navy Global Ocean Forecast System (Metzger et al. 2014). Bleck (2002) gives a detailed description of HYCOM physics. Thus, the numerical model is only briefly described here with an emphasis on those aspects that are relevant to this study.

HYCOM, a primitive equation general ocean circulation model, solves five prognostic equations: two for

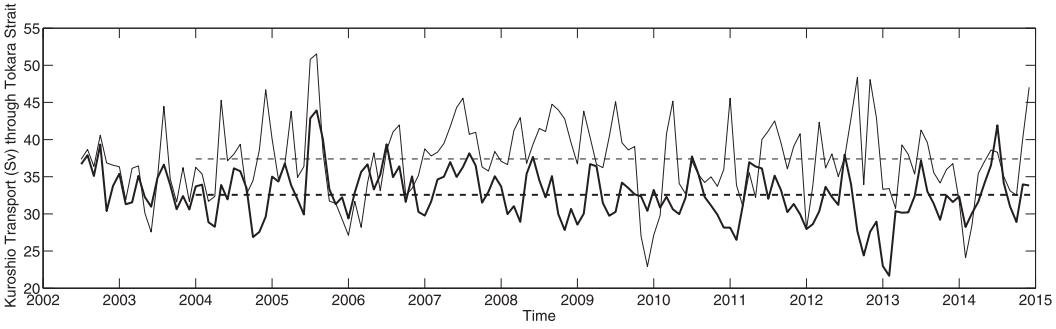

FIG. 1. Time series of monthly Kuroshio transport (Sv) through Tokara Strait for both experiments 1 [thin line; Eq. (1)] and 2 [thick line; Eq. (2)]. The corresponding dashed lines show the 11-yr (2004–14) mean transport (37.4 Sv for experiment 1; 32.6 Sv for experiment 2). The location of the transect at Tokara Strait is shown in Fig. 3.

horizontal velocity components, one for mass continuity equation, and two conservative equations that govern temperature and salinity. The prognostic equations are time integrated using a split-explicit treatment of the barotropic and baroclinic modes (Yu et al. 2015).

One of the advantages of HYCOM is its vertical coordinate system, of which there are three: z coordinates, terrain-following sigma coordinates, and isopycnal coordinates. None of these can be optimal everywhere in the global ocean by themselves (Chassignet et al. 2000), so HYCOM is configured to combine these three vertical coordinate systems. Hence, HYCOM maintains the significant advantages of an isopycnal model in the stratified ocean but allows coordinate surfaces to locally deviate from isopycnals to provide more vertical resolution near the surface within the mixed layer and in shallow coastal regions in order to better represent the upper-ocean physics (Chassignet et al. 2003).

The HYCOM horizontal resolution in this study is 0.08° (1/12.5°): ~9 km at the equator and ~6.5 km at midlatitude. The grid is uniform cylindrical from 78.64° to 66°S, Mercator between 66°S and 47°N, and includes a bipolar patch north of 47°N, providing ~3.5-km grid spacing at the North Pole. Thus, it is global eddy resolving. There are 41 hybrid vertical coordinate layers [nine layers more than the previous version used by Yu et al. (2015)] with potential density referenced to 2000 m. For this study, there is no data assimilation applied to the numerical simulations.

Two global HYCOM simulations are performed. The only difference between them is that experiment 1 does not include the effect of ocean surface currents in the wind stress bulk algorithm [Eq. (1)], whereas experiment 2 does [Eq. (2)]. The initialization state for experiments 1 and 2 is obtained in a two-step process: 1) a nonassimilative global HYCOM simulation is forced [according to Eq. (1)] with a 1993–2012 climatology from the 0.3125°-resolution National Centers for Environmental Prediction (NCEP) Climate Forecast System Reanalysis (CFSR; Saha et al. 2010) and run until the basinwide mean KE has reached statistical equilibrium, and 2) it is continued with hourly surface NCEP CFSR wind [according to Eq. (1)] and thermal forcing from 1993 to June 2002. Both experiments 1 and 2 are initialized at the end of June 2002 from step 2 and run for 12.5 yr forced with hourly NCEP CFSR forcing from July 2002 to the end of 2014. Both the globally integrated monthly mean KE and EKE (relative to the monthly mean) time series (not shown) show that it takes roughly 18 months for experiment 2 to adjust to the impulse associated with the modified wind stress formulation [Eq. (2)] and reach a steady state. The same conclusion can be drawn from the monthly mean Kuroshio transport (Fig. 1) time series. Thus, we only analyze results of the last 11 yr, from 2004 to 2014.

Since Sverdrup transport is a steady-state solution, we use the 11-yr average wind stress from experiments 1 and 2 to represent the steady state ($\_s$) of the wind stress, $\boldsymbol{\tau}_{c\_s}$ and $\boldsymbol{\tau}_{n\_s}$, respectively. The Kuroshio transport at steady state is represented by the 11-yr average. Volume transport through a zonal (meridional) HYCOM transect is calculated as the product of the meridional (zonal) depth-integrated barotropic velocity and the transect length. Because of the quadratic nature of wind stress, the steady state of the 10-m wind ($\mathbf{V}_{10\_s}$) cannot be achieved through averaging over the 11-yr period but rather is derived from $\boldsymbol{\tau}_{c\_s}$ as shown below:

$$|\mathbf{V}_{10\_s}| = \sqrt{\frac{|\boldsymbol{\tau}_{c\_s}|}{\rho_{\text{air}} C_d}}, \tag{3}$$

then the vector $\mathbf{V}_{10\_s}$ is derived from Eq. (1) as

$$\mathbf{V}_{10\_s} = \frac{\boldsymbol{\tau}_{c\_s}}{\rho_{\text{air}} C_d |\mathbf{V}_{10\_s}|}. \tag{4}$$

The quantities $|\mathbf{V}_{10\_s} - \mathbf{V}_{o\_s}|$ and $\mathbf{V}_{10\_s} - \mathbf{V}_{o\_s}$, where $\mathbf{V}_{o\_s}$ is the steady state of ocean surface currents, are derived in the same way from Eq. (2) as

$$|\mathbf{V}_{10\_s} - \mathbf{V}_{o\_s}| = \sqrt{\frac{|\boldsymbol{\tau}_{c\_n}|}{\rho_{\text{air}} C_d}}, \tag{5}$$

$$\mathbf{V}_{10\_s} - \mathbf{V}_{o\_s} = \frac{\boldsymbol{\tau}_{c\_n}}{\rho_{\text{air}} C_d |\mathbf{V}_{10\_s} - \mathbf{V}_{o\_s}|}, \tag{6}$$

and

$$\mathbf{V}_{o\_s} = \mathbf{V}_{10\_s} - \frac{\boldsymbol{\tau}_{c\_n}}{\rho_{\text{air}} C_d |\mathbf{V}_{10\_s} - \mathbf{V}_{o\_s}|}. \tag{7}$$

3. Difference in Sverdrup transport due to the effect of ocean currents: An analytical solution

The drag coefficient C_d in HYCOM is obtained from the Coupled Ocean–Atmosphere Response Experiment bulk algorithm (version 3.0; Fairall et al. 2003). It is expressed as simple polynomial functions of air–sea virtual temperature difference and 10-m winds (Kara et al. 2005). Kara et al. (2007a) demonstrate that including $\mathbf{V}_o$ in the C_d calculation reduces C_d by less than 1% when it is averaged over a long period (>1 month). Thus, C_d in both formulations [Eqs. (1) and (2)] can be treated as the same, since Sverdrup transport is a steady-state solution (long-term mean). Kara et al. (2007b) further reveal that the long-term mean of C_d can be treated as a constant to the leading order at midlatitudes (their Fig. 2). Thus, in the derivations below, we choose to use a constant C_d for the sake of simplicity, the same as Hughes and Wilson (2008).

The wind stress curl is a particularly important term in the wind-driven circulation since it defines the Sverdrup transport, the net amount of water transported meridionally. To understand the contribution of the 10-m winds to the Sverdrup transport, we rewrite the wind stress curl in terms of $\mathbf{V}_{10\_s}$ using Eq. (1):

$$M_c = \frac{\rho_{\text{air}} C_d}{\beta} \{|\mathbf{V}_{10\_s}| \nabla \times \mathbf{V}_{10\_s} + \nabla(|\mathbf{V}_{10\_s}|) \times \mathbf{V}_{10\_s}\}. \tag{8}$$

The first term inside the curly brackets on the right-hand side, wind vorticity torque, is simply the correlation of the wind speed and vorticity. It represents wind stress curl generation by 10-m wind vorticity through surface friction. The second term, wind speed gradient torque, contributes to wind stress curl when the wind direction is not parallel to the gradient of the wind speed. This term arises due to the quadratic nature of wind stress in which the stronger 10-m winds are retarded more than weaker winds at the sea surface. The Sverdrup transport is proportional to the sum of wind vorticity torque and speed gradient torque.

According to Eqs. (1) and (2), the wind stress difference induced by $\mathbf{V}_{o\_s}$ is

$$\boldsymbol{\tau}_{n\_s} - \boldsymbol{\tau}_{c\_s} = \rho_{air} C_d \{(|\mathbf{V}_{10\_s} - \mathbf{V}_{o\_s}| - |\mathbf{V}_{10\_s}|)\mathbf{V}_{10\_s} - |\mathbf{V}_{10\_s} - \mathbf{V}_{o\_s}|\mathbf{V}_{o\_s}\}. \tag{9}$$

The two terms in the curly brackets of Eq. (9) indicate the nonlinear interaction induced by $\mathbf{V}_{o\_s}$ due to the quadratic nature of wind stress. The first term is the wind stress difference caused by wind speed difference induced by $\mathbf{V}_{o\_s}$, which is shear speed ($|\mathbf{V}_{10\_s} - \mathbf{V}_{o\_s}|$) minus 10-m wind speed. The second term represents the wind stress difference arising from the wind stress direction change generated by ocean surface currents.

The Sverdrup transport difference induced by $\mathbf{V}_{o\_s}$ is

$$M_n - M_c = \frac{\nabla \times (\boldsymbol{\tau}_{n\_s} - \boldsymbol{\tau}_{c\_s})}{\beta}. \tag{10}$$

Substituting Eq. (9) into Eq. (10) and assuming $|\mathbf{V}_{o\_s}| \ll |\mathbf{V}_{10\_s}|$, we obtain

$$M_n - M_c = \frac{\rho_{\text{air}} C_d}{\beta} \{ - |\mathbf{V}_{o\_s}| \nabla \times \mathbf{V}_{10\_s} - \nabla(|\mathbf{V}_{o\_s}|) \times \mathbf{V}_{10\_s} - |\mathbf{V}_{10\_s}| \nabla \times \mathbf{V}_{o\_s} - \nabla(|\mathbf{V}_{10\_s}|) \times \mathbf{V}_{o\_s}\}. \tag{11}$$

The four terms on the right-hand side of Eq. (11) are results of nonlinear interactions between $\mathbf{V}_{o\_s}$ and $\mathbf{V}_{10\_s}$. They represent wind vorticity torque over ocean currents, ocean current speed torque over 10-m winds, ocean current vorticity torque over 10-m winds, and wind speed torque over ocean surface currents, respectively. The relative importance of these four terms is investigated in section 5a.

To quantify the Sverdrup transport difference induced by the effect of ocean surface currents, we estimate the ratio of $M_n - M_c$ to M_c. At steady state, 10-m winds (white arrows in Fig. 2a) and ocean surface currents (black arrows in Fig. 2b) have similar spatial scale for the midlatitude Pacific interior. A simple scale analysis reveals

$$\frac{M_n - M_c}{M_c} = -2 \frac{\mathbf{V}_{o\_s}}{\mathbf{V}_{10\_s}}. \tag{12}$$

The negative sign on the right-hand side of the equation suggests that the ocean surface current dependence in the wind stress formulation reduces the Sverdrup transport when $\mathbf{V}_{o\_s}$ is in the same direction as the 10-m winds. But

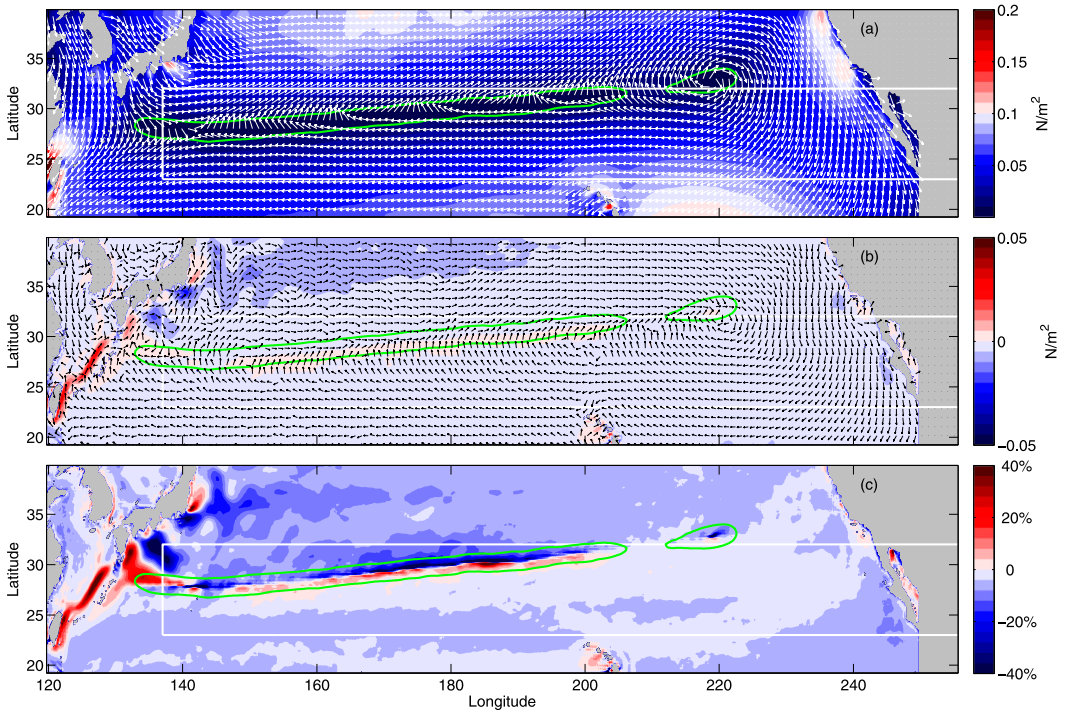

FIG. 2. (a) Mean NCEP CFSR wind stress magnitude (N m^{-2}; $|\boldsymbol{\tau}_{c\_s}|$, without the effect of ocean currents) averaged over 2004 to 2014 in the North Pacific. The wind direction is shown with white arrows. (b) Mean wind stress magnitude difference ($|\boldsymbol{\tau}_{n\_s}| - |\boldsymbol{\tau}_{c\_s}|$) induced by $\mathbf{V}_{o\_s}$. The direction of $\mathbf{V}_{o\_s}$ is shown with black arrows. (c) The ratio of mean wind stress magnitude difference ($|\boldsymbol{\tau}_{n\_s}| - |\boldsymbol{\tau}_{c\_s}|$) induced by $\mathbf{V}_{o\_s}$ to the wind stress magnitude without the effect of ocean currents ($|\boldsymbol{\tau}_{c\_s}|$). The white box defines the region of interest from 23° to 32°N and 137°E to the American coast. The green lines are the 0.01-Pa isoline and represent the weak wind stress zone in the midlatitude North Pacific.

when ocean surface currents are opposite to the 10-m winds, the $\mathbf{V}_{o\_s}$ dependence can increase Sverdrup transport. Empirical estimations based on surface Ekman current theory suggest that the typical value of $|\mathbf{V}_o|/|\mathbf{V}_{10}|$ is about 3% (Colling 2001). This gives us an analytical reduction rate of 6% in Sverdrup transport when Ekman dynamics dominate.

4. Model results

a. Wind stress magnitude

The 11-yr (2004 to 2014) mean wind stress $\boldsymbol{\tau}_{c\_s}$, calculated from the NCEP CFSR wind velocity using Eq. (1), is shown in Fig. 2a. A weak wind stress zone (<0.01 Pa) spans the midlatitude North Pacific from 28°N, 130°E to 32°N, 137°W, as shown by the dark blue region confined within the green contour lines, where the wind (white arrows) switches directions. Wind stress magnitude increases gradually toward the south and north of it. The Kuroshio and its extension are apparent in the mean wind stress magnitude difference between experiments 2 and 1 ($|\boldsymbol{\tau}_{n\_s}| - |\boldsymbol{\tau}_{c\_s}|$) shown in Fig. 2b. This difference can be expressed in terms of $\mathbf{V}_{10\_s}$ and $\mathbf{V}_{o\_s}$:

$$|\boldsymbol{\tau}_{n\_s}| - |\boldsymbol{\tau}_{c\_s}| = \rho_{\text{air}} C_d (|\mathbf{V}_{o\_s}|^2 - 2|\mathbf{V}_{o\_s}||\mathbf{V}_{10\_s}|\cos\theta), \quad (13)$$

where θ is the angle between $\mathbf{V}_{o\_s}$ and $\mathbf{V}_{10\_s}$. This equation suggests that as long as $\theta > \cos^{-1}[|\mathbf{V}_{o\_s}|/(2|\mathbf{V}_{10\_s}|)]$, $|\boldsymbol{\tau}_{n\_s}|$ is greater than $|\boldsymbol{\tau}_{c\_s}|$. Since the surface speed of the Kuroshio and its extension is much stronger than the wind-generated surface currents in the open ocean, they modify the local wind stress magnitude significantly. The impact is opposite to the east and west of 133°E. The $|\boldsymbol{\tau}_{n\_s}|$ is greater than $|\boldsymbol{\tau}_{c\_s}|$ to the west of 133°E: through the East Taiwan Channel (ETC), inside the ECS, and to the east of Kyushu, Japan. To the east of 133°E, the presence of the Kuroshio and its extension decreases the wind stress magnitude in general. This is simply because the mean wind stress is generally against the Kuroshio to the west of 133°E, while it typically follows the Kuroshio and its extension to the east (Fig. 3). A similar wind stress pattern was reported previously using a different wind stress climatology (Fig. 4b of Nakamura et al. 2007; Fig. 9 of

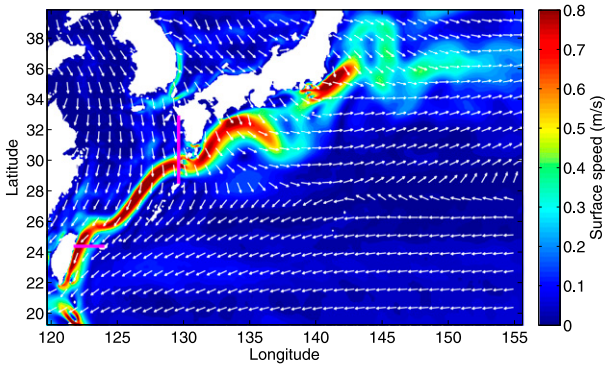

FIG. 3. The steady-state ocean surface current speed (m s^{-1}; $|\mathbf{V}_{o\_s}|$) from HYCOM experiment 2 with the effect of the ocean currents in the wind stress bulk algorithm. The wind direction associated with the steady-state wind stress $\boldsymbol{\tau}_{c\_s}$ is shown with white arrows. The magenta lines show transects at the ETC and Tokara Strait where HYCOM transport is computed.

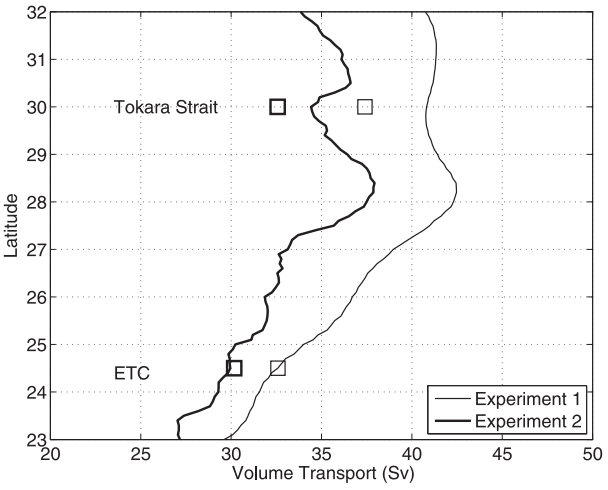

FIG. 4. The zonally integrated Sverdrup transport (Sv) as a function of latitude and computed for the white box shown in Fig. 2 from the two HYCOM simulations. Thick line shows results from the HYCOM experiment 2 with ocean currents in the wind stress formulation, while the thin line shows results from the HYCOM experiment 1, without ocean currents in the wind stress formulation. The corresponding simulated 11-yr mean Kuroshio transports (squares) through the magenta transects shown in Fig. 3 are also shown.

Nakamura et al. 2010; Fig. 10 of Hao et al. 2012; Fig. 10 of Yu et al. 2015).

The relative importance of $\mathbf{V}_{o\_s}$ on the wind stress magnitude is examined through the ratio of $|\boldsymbol{\tau}_{n\_s}| - |\boldsymbol{\tau}_{c\_s}|$ to $|\boldsymbol{\tau}_{c\_s}|$ in Fig. 2c. There are two main regions in the midlatitude North Pacific where ocean currents are important to the wind stress magnitude. One region is along the Kuroshio and extension, where the ocean surface currents are strong, and the other region is along the center of the weak wind stress zone (green contours in Fig. 2). The term $\mathbf{V}_{o\_s}$ also switches direction along the weak wind zone and shifts slightly southward (arrows in Fig. 2b vs Fig. 2a). To the southern part of the weak wind zone, $\mathbf{V}_{o\_s}$ is against the wind, while it mainly follows the wind in the northern half and thus mainly increases wind stress magnitude to the south (Figs. 2b,c) and decreases it to the north. The effect of ocean currents can increase/decrease the wind stress magnitude by more than 40% in these two regions.

b. *Sverdrup transport and Kuroshio transport in the East China Sea*

Hautala et al. (1994) demonstrate that the subtropical North Pacific is in Sverdrup balance along 24°N from the eastern boundary (North America coast) to about 137°E, and the estimated Sverdrup transport agrees well with the observed Kuroshio transport through the ETC. Because the Kuroshio enters the ECS through the ETC and exits through the Tokara Strait (Fig. 3, magenta lines), we define our study area from 23° to 32°N and from the American coast to 137°E (white box in Fig. 2) in accord with Hautala et al. (1994).

The zonally integrated Sverdrup transport is calculated within the white box using the two different wind stresses from experiments 1 and 2 ($\boldsymbol{\tau}_{c\_s}$ and $\boldsymbol{\tau}_{n\_s}$) and illustrated in Fig. 4 as a function of latitude. Both transports show similar latitude dependency, which increases from 23° to ~28.5°N and then decreases from 28.5° to 30°N. The Sverdrup transport in experiment 2 (with ocean currents in the wind stress formulation, thick line) is lower than that in experiment 1 (without ocean currents in the wind stress formulation, thin line) at all latitudes, in good agreement with the analytical solution we found in section 3. The corresponding simulated Kuroshio transport (squares in Fig. 4) through the ETC [32.6/30.2 Sv (1 Sv $\equiv 10^6$ m^3 s^{-1}) in experiments 1/2] and Tokara Strait (37.4/32.6 Sv in experiments 1/2) shows the same tendency. The Kuroshio transport through the ETC is almost the same as the Sverdrup transport (32.6/30.0 Sv in experiments 1/2; Table 1) at the same latitude (24.4°N) for both experiments, consistent with Hautala et al. (1994) in that the subtropical North Pacific is in Sverdrup balance along 24°N. However, the simulated Kuroshio transport through Tokara Strait is lower than the Sverdrup transport (40.8/34.5 Sv in experiments 1/2; Table 1) at the same latitude in both experiments. This is because the Kuroshio is not the only western boundary current there. Hautala et al. (1994) propose a scenario where the Sverdrup balance is also valid in the Philippine Sea (from the Philippine's coast to 137°E) and a mean northward flow exists in the western Philippine Sea. Their hypothesis is confirmed by

TABLE 1. Kuroshio volume transport (Sv) through the East Taiwan Channel and Tokara Strait and the Sverdrup transport at the corresponding latitude from the HYCOM experiment 1, without ocean currents in the wind stress formulation $\boldsymbol{\tau}_{c\_s}$, and experiment 2, with ocean currents in the wind stress formulation $\boldsymbol{\tau}_{n\_s}$. The difference of Sverdrup transport, Kuroshio transport, and Ekman transport induced by $\mathbf{V}_{o-s}$ are also shown.

Location		$\boldsymbol{\tau}_{c\_s}$	$\boldsymbol{\tau}_{n\_s}$	$\boldsymbol{\tau}_{n\_s} - \boldsymbol{\tau}_{c\_s}$	Ekman transport $(\boldsymbol{\tau}_{n\_s} - \boldsymbol{\tau}_{c\_s})$
East Taiwan Channel	Sverdrup	32.6	30.0	−2.6	−0.03
	Kuroshio	32.6	30.2	−2.5	
Tokara Strait	Sverdrup	40.8	34.5	−6.3	−0.01
	Kuroshio	37.4	32.6	−4.8	

observations (Zhu et al. 2003; Ichikawa et al. 2004; Zhu et al. 2005) that found the Ryukyu Current System to the east of Ryukyu Islands Arc. The Sverdrup transport at Tokara Strait's latitude is attributed to both the Kuroshio and the Ryukyu Current Systems.

Including ocean currents in the wind stress formulation reduces the zonally integrated Sverdrup transport by 8%–17% (Fig. 5, black line) from 23° to 32°N. The reduction rate of the 10-yr mean Kuroshio transport (Fig. 5, square) through the ETC and Tokara Strait is 8.0% and 12.8%, respectively, in good agreement with the Sverdrup transport reduction rate along the corresponding latitude, 7.4% and 15.4%. This indicates that the Kuroshio transport reduction due to the inclusion of surface currents in wind stress formulation is mainly a response to the remote forcing in the Pacific interior. Plugging in the steady-state surface current $\mathbf{V}_{o\_s}$ and 10-m wind $\mathbf{V}_{10\_s}$ values in Eq. (12) gives a 6.2% and 15.2% reduction (solid dots in Fig. 5) of Sverdrup transport along the latitude of ETC and Tokara Strait, respectively, which confirms that the model results are consistent with our analytical solution.

The Sverdrup transport difference ($M_n - M_c$; experiment 2 − experiment 1) is shown in Fig. 6. A positive value indicates Sverdrup transport reduction by including ocean currents in wind stress formulation. It clearly shows that the Kuroshio and its extension make the most significant contribution to the Sverdrup transport difference due to its strong currents. Nonlinear dynamics likely play an important role in these regions, which violate the assumption Sverdrup originally envisioned (Gray and Riser 2014). Thus, our study area is carefully chosen to avoid these regions (white box, Fig. 6).

c. *Local effect in the East China Sea*

Because of its strong surface current and narrow front, the Kuroshio modifies the local wind stress magnitude significantly (Fig. 2b). Local effects due to the change of wind stress by $\mathbf{V}_{o\_s}$ may come into play in

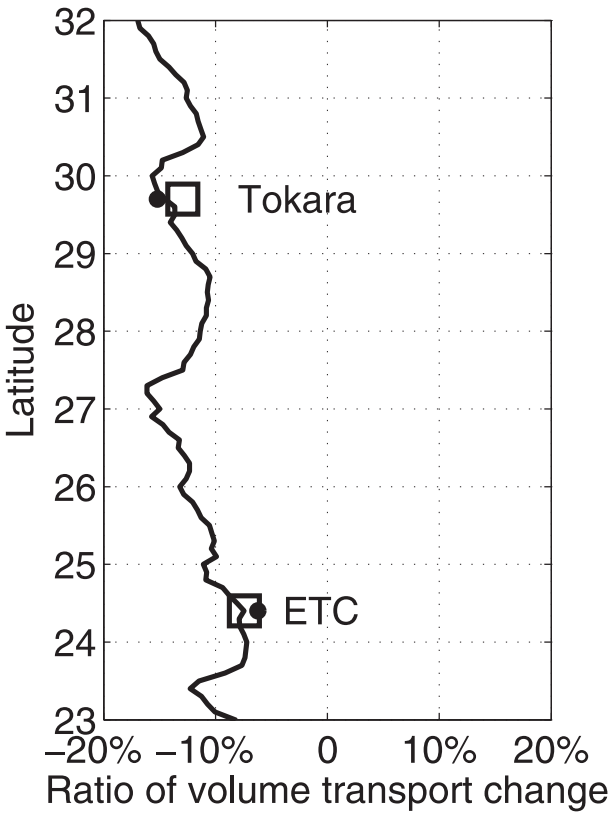

FIG. 5. The zonally integrated Sverdrup transport change (%, as a percentile to M_c) as a function of latitude due to the effect of ocean currents in the wind stress formulation. The corresponding Kuroshio transport difference and $-2(\mathbf{V}_{o\_s}/\mathbf{V}_{10\_s})$ from the HYCOM simulations are shown with squares and solid dots, respectively.

our estimates of Kuroshio transport in two ways: 1) the top drag and the reduction of wind work caused by $\mathbf{V}_{o\_s}$ would slow the current, and 2) the flow instability and Kuroshio interaction with the topography lead to the formation of mesoscale eddies and meanders, whose surface currents can significantly modify the Ekman pumping via their surface vorticity gradients (Gaube et al. 2015; Seo et al. 2016). However, as shown below, these local effects are negligible in the change of Kuroshio transport compared to its response to the remote forcing in the Pacific interior.

The Sverdrup transport is a steady-state solution. At steady state, the transient eddies vanish and the energy has to balance. The surface currents have two components: the geostrophic current and the surface Ekman velocity. There is no net work done by Ekman velocities because the wind work by Ekman velocity must be dissipated within the Ekman layer for a steady state to exist (Stern 1975). Only wind work generated by geostrophic currents ($\boldsymbol{\tau} \cdot \mathbf{V}_g$, where $\mathbf{V}_g$ is the geostrophic current) needs to be considered for the local effect of $\mathbf{V}_{o\_s}$ on Kuroshio transport.

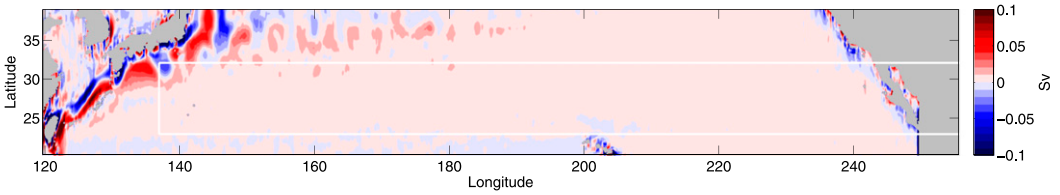

FIG. 6. The Sverdrup transport (Sv) difference ($M_n - M_c$) in the North Pacific. The white box highlights the study area.

According to Fofonoff (1980), there exists a very simple steady-state relation:

$$\boldsymbol{\tau} \cdot \mathbf{V}_g = \frac{1}{\rho_o} M_e \nabla_h P, \tag{14}$$

where M_e is the Ekman mass transport, $\nabla_h P$ is the horizontal pressure gradient, and ρ_o is the density of the ocean. It tells us that the wind stress work on the surface geostrophic currents is the same as the pressure work done by Ekman transport up against the pressure gradient. So the local effect of changing wind stress/wind work by $\mathbf{V}_{o\_s}$ can be reflected by the Ekman transport difference at steady state.

The Ekman mass transport is $M_e = -(\mathbf{k}\times\boldsymbol{\tau})/f$, where $\mathbf{k}$ is the vertical unit vector. Since it is to the right of the wind stress direction (Northern Hemisphere), we only calculate the Ekman transport arising from the wind stress difference normal to the Kuroshio mean path, which are −0.03 and −0.01 Sv (Table 1) through ETC and Tokara Strait, respectively. These are negligible compared with the reduction of Sverdrup transport and Kuroshio transport (Table 1), as discussed in the previous section. Thus, the local effect of changing wind stress/wind work by $\mathbf{V}_{o\_s}$ is not important for the Kuroshio volume transport change estimated in the previous section.

5. Discussion and conclusions

In this study, we have derived an analytical solution to calculate the difference in Sverdrup transport due to the inclusion of ocean currents in the wind stress formulation. It demonstrates that ocean currents reduce the Sverdrup transport when they are in the same direction as the winds.

Two HYCOM numerical simulations were run for a 12.5-yr period (from July 2002 to 2014) with (experiment 2) and without (experiment 1) ocean currents in the wind stress formulation. Model results from the last 11 yr (2004–14) are analyzed when both numerical simulations are in steady state. The model results indicate a 2.5-/4.8-Sv (Table 1) reduction of Kuroshio transport through the ETC/Tokara Strait when ocean currents are included in the wind stress formulation, being consistent with the analytical solution. The model results also reveal that the 6% transport reduction rate obtained from the scale analysis of the analytical solution is the lower limit in the midlatitude North Pacific, and the Sverdrup transport reduction rate can be as large as 17%, where strong ocean currents exist. Similar to what we observed for the Kuroshio transport, the model-simulated volume transport of the Gulf Stream is also weaker when ocean currents are included in the wind stress bulk algorithm. The reduction in Gulf Stream volume transport through the Florida Strait is 7.2%, also in good agreement with the analytical solution.

Consistent with Dawe and Thompson (2006), we find that wind stress magnitude changes significantly along the Kuroshio and its extension due to the effect of strong ocean surface currents. The rate of wind stress magnitude change depends on the relative strength of the ocean surface currents to the 10-m winds. Thus, the rate of wind stress magnitude change is also significant along the weak wind zone in the midlatitude region of the North Pacific, where the wind switches direction and wind stress is less than 0.01 Pa.

a. Relative importance of the four terms in Eq. (11)

Four nonlinear terms contribute to the wind stress curl difference in Eq. (11), which determines the difference in Sverdrup transport due to the inclusion of ocean currents in wind stress formulations. To understand their relative importance, they are zonally integrated and then divided by the Sverdrup transport difference between experiments 2 and 1 ($M_n - M_c$) to calculate the reduction rate as shown in Fig. 7.

First, the two vorticity torque terms [terms 1 and 3 in Eq. (11); thick and thin lines, respectively, in Fig. 7] are all positive, which reduces Sverdrup transport when including ocean currents in wind stress formulation. This is because the wind vorticity and surface current vorticity are both mainly negative in the study area (Figs. 2a,b). And thus the two vorticity torque terms always reduces Sverdrup transport.

Second, the speed torque [term 2 and term 4 in Eq. (11); thick and thin dashed lines, respectively, in Fig. 7] terms

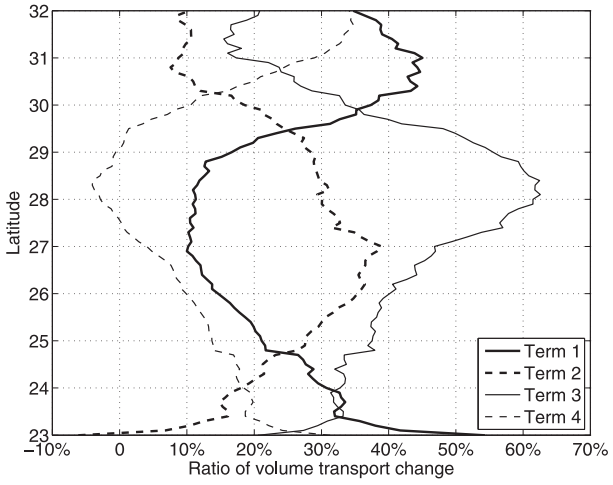

FIG. 7. The relative importance of the four nonlinear terms on the right-hand side of Eq. (11) as a function of latitude due to the effect of ocean currents in the wind stress formulation. Terms 1 to 4 are $-(\rho_{\text{air}}C_d|\mathbf{V}_{o\_s}|\nabla\times\mathbf{V}_{10\_s})/(M_n-M_c)$, $-[\rho_{\text{air}}C_d\nabla(|\mathbf{V}_{o\_s}|)\times\mathbf{V}_{10\_s}]/(M_n-M_c)$, $-(\rho_{\text{air}}C_d|\mathbf{V}_{10\_s}|\nabla\times\mathbf{V}_{o\_s})/(M_n-M_c)$, and $-[\rho_{\text{air}}C_d\nabla(|\mathbf{V}_{10\_s}|)\times\mathbf{V}_{o\_s}]/(M_n-M_c)$, respectively.

can be negative, which increases Sverdrup transport when including ocean currents in wind stress formulation. The sign of the two speed torque terms depends on the relative direction of the speed gradient to the winds [term 2 in Eq. (11)] or ocean currents [term 4 in Eq. (11)]. If the speed gradient is to the left of the winds or ocean currents, it reduces the Sverdrup transport and vice versa. From Fig. 2a, the wind speed gradient is mainly northward (southward) to the north (south) of the weak wind zone (green contour lines). Thus, the wind speed gradient is mainly to the left of the ocean currents (Fig. 2b, white arrows) outside of the weak wind zone. But inside the weak wind zone, the wind speed gradient can be to the right side of the ocean currents due to the direction shifting of ocean currents. This would increase the Sverdrup transport when including ocean currents in the wind stress formulation and result in a negative value of term 4, $-[\rho_{\text{air}}C_d\nabla(|\mathbf{V}_{10\_s}|)\times\mathbf{V}_{o\_s}]/(M_n-M_c)$ (wind speed torque over ocean surface currents), between 27.5° and 29°N.

Third, the shape of terms 1 and 4 and terms 2 and 3 is really similar. These terms arise by a different mechanism: terms 1 and 4 are torques generated by winds, while terms 2 and 3 are torques determined by ocean currents. Terms 1 and 3 (vorticity torque) make more contribution to the reduction of Sverdrup transport than terms 4 and 2 (speed torque) at any given latitude in the study area, respectively. Term 2 between 23° and 23.3°N and between 30.5° and 32°N and term 4 between 26° and 30°N make less than a 10% contribution to the Sverdrup transport difference in the corresponding region and thus are negligible. But overall, these four terms have similar magnitude and are all important to the Sverdrup transport difference.

b. Kuroshio pathway between 130° and 135°E

Upon exiting Tokara Strait, the Kuroshio turns sharply northeastward and closely follows the Japanese coast as far as Shikoku (Fig. 1 of Kawabe 1995), regardless of which downstream pathway it takes [nonlarge meander or large meander as described by Kawabe (1985)]. Surface speed contours from both experiments are used to define the Kuroshio pathway each year and shown every 3 yr in Fig. 8. Experiment 2 generates realistic Kuroshio pathways between 130° and 135°N for all 11 yr of the 2004–14 simulation (red lines). However, experiment 1 shows an unrealistic zonally oriented Kuroshio pathway between 130° and 135°N from 2009 to 2014 (black lines). Douglass et al. (2012) reported a similar zonally oriented Kuroshio pathway east of Tokara Strait (their Fig. 2a) when they ran the Parallel Ocean Program model with 0.1° resolution in the zonal direction and 0.1° x cos(latitude) in the meridional direction. Their simulation was forced by a climatology blending NCEP reanalysis products and remote sensing products. Ocean currents were not considered in their wind stress formulations.

One possible explanation for the unrealistic Kuroshio pathway between 130° and 135°N is attributed to the excessive inertial currents through the Tokara Strait, a result also noted in Hurlburt et al. (1996, their plate 6c). Our results seem to support this explanation. By including the ocean currents in the wind stress formulation, the transport through Tokara Strait is reduced by 12.8%, which leads to a less energetic Kuroshio through the strait.

Another possible explanation is related to the trigger meander (Endoh and Hibiya 2001; Usui et al. 2008a) and interaction between eddies, the Kuroshio, and topography (Usui et al. 2008b; Endoh and Hibiya 2009), leading to the large meander south of Japan. This zonally oriented pathway was referred to as a large meander in Douglass et al. (2012). And it indeed looks like an extended larger meander between 130° and 140°N (Fig. 8). In our study, experiment 2 has lower Kuroshio volume transport entering/exiting the ECS, which leads to lower volume transport in the Kuroshio Extension. As the result, the velocity of the Kuroshio Extension is lower, and the velocity shear is also weaker. The reduction in current velocity and shear reduces the flow instability and hence lowers the number of triggering meander and mesoscale eddies. We observe ~20%

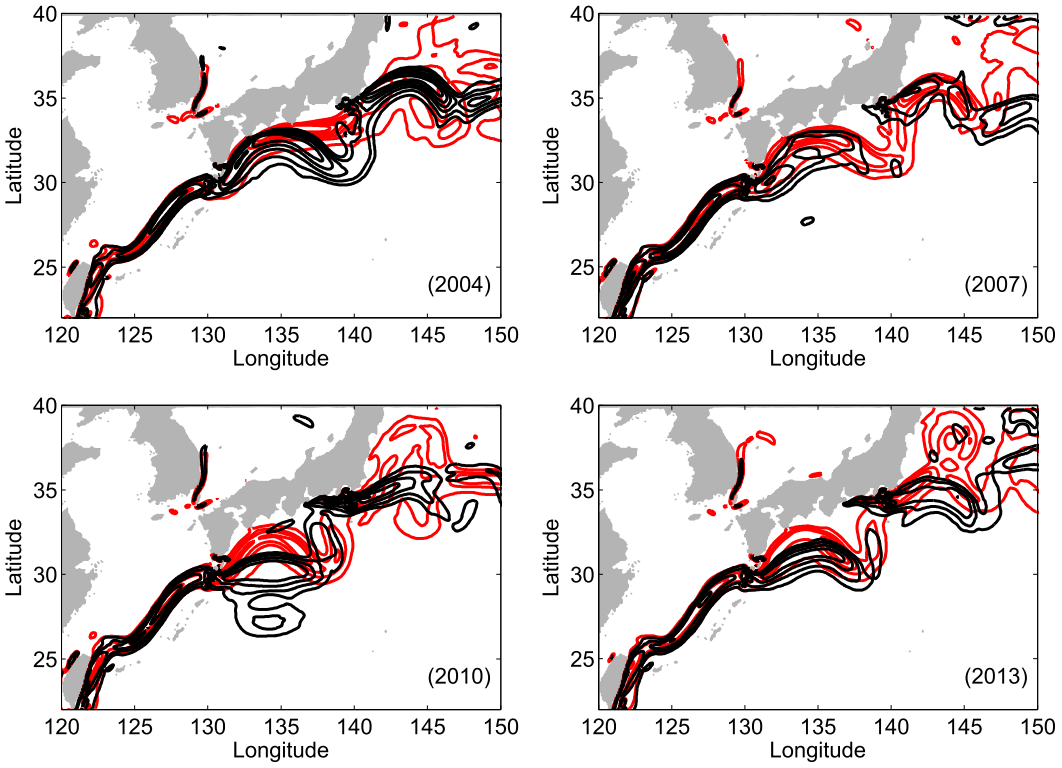

FIG. 8. Annual-mean Kuroshio pathway defined by the surface speed contours in 2004, 2007, 2010, and 2013. Black (red) isolines of ocean surface speed show the Kuroshio pathway from the HYCOM experiment 1 (2) without (with) the effect of the ocean currents in the wind stress bulk algorithm.

fewer number of all eddies in the Kuroshio Extension in experiment 2 than experiment 1, consistent with previous research (J. Shriver 2016, personal communication). Furthermore, these eddies are shorter lived, smaller in size, and weaker in intensity as a result of the top drag (Dewar and Flierl 1987). Thus, statistically, there is a higher chance for experiment 1 to form the extended large meander.

The Kuroshio pathway and its eddies affect everything from fisheries to marine navigation to air–sea interaction in the region south of Japan. The variability of the Kuroshio pathway and volume transport through Tokara Strait are also thought to be crucial in understanding the Kuroshio meander variations south of Japan (Masuda 1982; Chao 1984; Yasuda et al. 1985; Yamagata and Umatani 1989; Kawabe 1995; Hurlburt et al. 1996). Although the reason for the unrealistic Kuroshio pathway between 130° and 135°N remains unclear, the results of this study have suggested a potential significant impact of including ocean currents in the wind stress formulation on the realistic simulation of the Kuroshio pathway between 130° and 135°N in general ocean circulation models. More research and longer-term statistics are needed to study the mechanism that leads to realistic Kuroshio pathway. Since the ocean and the atmosphere are a fully coupled system, the variation of the Kuroshio pathway also affects the surface wind patterns (Nonaka and Xie 2003; Xie 2004; Small et al. 2008). Coupled atmosphere–ocean models are needed to further understand the impact of including ocean currents in the wind stress formulation.

Acknowledgments. The authors thank the editor and two anonymous reviewers for their input to improve the original manuscript. Both Z. Yu and E. J. Metzger were funded by the "6.1 Kuroshio and Ryukyu Current Dynamics" project sponsored by the Office of Naval Research under Program Element 0601135N. Z. Yu was also partially supported by the Karle's Research Fellowship through the Naval Research Laboratory. Y. Fan was funded by the "6.1 The Effect of Langmuir Turbulence in Upper Ocean Mixing" project sponsored by the Office of Naval Research. Computer time was provided by the Department of Defense (DoD) High-Performance Computing Modernization Program, and the simulations were performed on the Cray XC30 (Shepard) at the Navy DoD Supercomputing Resources Center, Stennis Space Center, Mississippi. It has been approved for public release and distribution is unlimited.

REFERENCES

Bleck, R., 2002: An oceanic general circulation model framed in hybrid isopycnic-Cartesian coordinates. *Ocean Modell.*, **4**, 55–88, doi:10.1016/S1463-5003(01)00012-9.

Chao, S.-Y., 1984: Bimodality of the Kuroshio. *J. Phys. Oceanogr.*, **14**, 92–103, doi:10.1175/1520-0485(1984)014<0092:BOTK>2.0.CO;2.

Chassignet, E. P., and Coauthors, 2000: DAMEE_NAB: The base experiments. *Dyn. Atmos. Oceans*, **32**, 155–184, doi:10.1016/S0377-0265(00)00046-4.

——, L. T. Smith, G. R. Halliwell, and R. Bleck, 2003: North Atlantic simulations with the Hybrid Coordinate Ocean Model (HYCOM): Impact of the vertical coordinate choice, reference pressure, and thermobaricity. *J. Phys. Oceanogr.*, **33**, 2504–2526, doi:10.1175/1520-0485(2003)033<2504:NASWTH>2.0.CO;2.

Chelton, D. B., and S.-P. Xie, 2010: Coupled ocean–atmosphere interaction at oceanic mesoscales. *Oceanography*, **23**, 52–69, doi:10.5670/oceanog.2010.05.

——, and Coauthors, 2001: Observations of coupling between surface wind stress and sea surface temperature in the eastern tropical Pacific. *J. Climate*, **14**, 1479–1498, doi:10.1175/1520-0442(2001)014<1479:OOCBSW>2.0.CO;2.

——, M. G. Schlax, M. H. Freilich, and R. F. Milliff, 2004: Satellite measurements reveal persistent small-scale features in ocean winds. *Science*, **303**, 978–983, doi:10.1126/science.1091901.

Colling, A., 2001: *Ocean Circulation.* 2nd ed. Butterworth Heinemann, 286 pp.

Cornillon, P., and K.-A. Park, 2001: Warm core ring velocities inferred from NSCAT. *Geophys. Res. Lett.*, **28**, 575–578, doi:10.1029/2000GL011487.

Dawe, J. T., and L. Thompson, 2006: Effect of ocean surface currents on wind stress, heat flux, and wind power input to the ocean. *Geophys. Res. Lett.*, **33**, L09604, doi:10.1029/2006GL025784.

Dewar, W. K., and G. R. Flierl, 1987: Some effects of the wind on rings. *J. Phys. Oceanogr.*, **17**, 1653–1667, doi:10.1175/1520-0485(1987)017<1653:SEOTWO>2.0.CO;2.

Douglass, E. M., S. R. Jayne, F. O. Bryan, S. Peacock, and M. Maltrud, 2012: Kuroshio pathways in a climatologically forced model. *J. Oceanogr.*, **68**, 625–639, doi:10.1007/s10872-012-0123-y.

Duhaut, T. H. A., and D. N. Straub, 2006: Wind stress dependence on ocean surface velocity: Implications for mechanical energy input to ocean circulation. *J. Phys. Oceanogr.*, **36**, 202–211, doi:10.1175/JPO2842.1.

Eden, C., and H. Dietze, 2009: Effects of mesoscale eddy/wind interactions on biological new production and eddy kinetic energy. *J. Geophys. Res.*, **114**, C05023, doi:10.1029/2008JC005129.

Endoh, T., and T. Hibiya, 2001: Numerical simulation of the transient response of the Kuroshio leading to the large meander formation south of Japan. *J. Geophys. Res.*, **106**, 26 833–26 850, doi:10.1029/2000JC000776.

——, and ——, 2009: Interaction between the trigger meander of the Kuroshio and the abyssal anticyclone over Koshu Seamount as seen in the reanalysis data. *Geophys. Res. Lett.*, **36**, L18604, doi:10.1029/2009GL039389.

Fairall, C. W., E. F. Bradley, J. E. Hare, A. A. Grachev, and J. B. Edson, 2003: Bulk parameterization of air–sea fluxes: Updates and verification for the COARE algorithm. *J. Climate*, **16**, 571–591, doi:10.1175/1520-0442(2003)016<0571:BPOASF>2.0.CO;2.

Fofonoff, N. P., 1980: The Gulf Stream system. *Evolution of Physical Oceanography: Scientific Surveys in Honor of Henry Stommel*, B. A. Warren and C. Wunsch, Eds., MIT Press, 112–139.

Frenger, I., N. Gruber, R. Knutti, and M. Munnich, 2013: Imprint of Southern Ocean eddies on winds, clouds and rainfall. *Nat. Geosci.*, **6**, 608–612, doi:10.1038/ngeo1863.

Gaube, P. D., D. B. Chelton, R. M. Samelson, M. G. Schlax, and L. W. O'Neill, 2015: Satellite observations of mesoscale eddy-induced Ekman pumping. *J. Phys. Oceanogr.*, **45**, 104–132, doi:10.1175/JPO-D-14-0032.1.

Gray, A. R., and S. C. Riser, 2014: A global analysis of Sverdrup balance using absolute geostrophic velocities from Argo. *J. Phys. Oceanogr.*, **44**, 1213–1229, doi:10.1175/JPO-D-12-0206.1.

Hao, J., Y. Chen, F. Wang, and P. Lin, 2012: Seasonal thermocline in the China Seas and northwestern Pacific Ocean. *J. Geophys. Res.*, **117**, C02022, doi:10.1029/2011JC007246.

Hautala, S., D. Roemmich, and W. J. Schmitz Jr., 1994: Is the North Pacific in Sverdrup balance along 24°N? *J. Geophys. Res.*, **99**, 16 041–16 052, doi:10.1029/94JC01084.

Hughes, C. W., and C. Wilson, 2008: Wind work on the geostrophic ocean circulation: An observational study of the effect of small scales in the wind stress. *J. Geophys. Res.*, **113**, C02016, doi:10.1029/2007JC004371.

Hughes, G. O., A. M. Hogg, and R. W. Griffiths, 2009: Available potential energy and irreversible mixing in the meridional overturning circulation. *J. Phys. Oceanogr.*, **39**, 3130–3146, doi:10.1175/2009JPO4162.1.

Hurlburt, H. E., A. J. Wallcraft, W. J. Schmitz Jr., P. J. Hogan, and E. J. Metzger, 1996: Dynamics of the Kuroshio/Oyashio Current System using eddy-resolving models of the North Pacific Ocean. *J. Geophys. Res.*, **101**, 941–976, doi:10.1029/95JC01674.

Ichikawa, H., H. Nakamura, A. Nishina, and M. Higashi, 2004: Variability of northeastward current southeast of northern Ryukyu Islands. *J. Oceanogr.*, **60**, 351–363, doi:10.1023/B:JOCE.0000038341.27622.73.

Kara, A. B., H. E. Hurlburt, and A. J. Wallcraft, 2005: Stability-dependent exchange coefficients for air–sea fluxes. *J. Atmos. Oceanic Technol.*, **22**, 1080–1094, doi:10.1175/JTECH1747.1.

——, E. J. Metzger, and M. A. Bourassa, 2007a: Ocean current and wave effects on wind stress drag coefficient over the global ocean. *Geophys. Res. Lett.*, **34**, L01604, doi:10.1029/2006GL027849.

——, A. J. Wallcraft, E. J. Metzger, and H. E. Hurlburt, 2007b: Wind stress drag coefficient over the global ocean. *J. Climate*, **20**, 5856–5864, doi:10.1175/2007JCLI1825.1.

Kawabe, M., 1985: Sea level variations at the Izu Islands and typical stable paths of the Kuroshio. *J. Oceanogr. Soc. Japan*, **41**, 307–326, doi:10.1007/BF02109238.

——, 1995: Variations of current path, velocity, and volume transport of the Kuroshio in relation with the large meander. *J. Phys. Oceanogr.*, **25**, 3103–3117, doi:10.1175/1520-0485(1995)025<3103:VOCPVA>2.0.CO;2.

Kelly, K. A., S. Dickinson, M. J. McPhaden, and G. C. Johnson, 2001: Ocean currents evident in satellite wind data. *Geophys. Res. Lett.*, **28**, 2469–2472, doi:10.1029/2000GL012610.

Luo, J.-J., S. Masson, R. Roeckner, G. Madec, and T. Yamagata, 2005: Reducing climatology bias in an ocean–atmosphere CGCM with improved coupling physics. *J. Climate*, **18**, 2344–2360, doi:10.1175/JCLI3404.1.

Masuda, A., 1982: An interpretation of the bimodal character of the stable Kuroshio path. *Deep-Sea Res.*, **29**, 471–484, doi:10.1016/0198-0149(82)90071-1.

Metzger, E. J., and Coauthors, 2014: US Navy operational global ocean and Arctic ice prediction systems. *Oceanography*, **27**, 32–43, doi:10.5670/oceanog.2014.66.

Nakamura, H., H. Ichikawa, and A. Nishina, 2007: Numerical study of the dynamics of the Ryukyu Current System. *J. Geophys. Res.*, **112**, C04016, doi:10.1029/2006JC003595.

——, M. Monaka, and H. Sasaki, 2010: Seasonality of the Kuroshio path destabilization phenomenon in the Okinawa Trough: A numerical study of its mechanism. *J. Phys. Oceanogr.*, **40**, 530–550, doi:10.1175/2009JPO4156.1.

Nonaka, M., and S. Xie, 2003: Covariations of sea surface temperature and wind over the Kuroshio and its extension: Evidence for ocean-to-atmosphere feedback. *J. Climate*, **16**, 1404–1413, doi:10.1175/1520-0442(2003)16<1404:COSSTA>2.0.CO;2.

O'Neill, L. W., S. K. Esbensen, N. Thum, R. M. Samelson, and D. B. Chelton, 2010: Dynamical analysis of the boundary layer and surface wind responses to mesoscale SST perturbations. *J. Climate*, **23**, 559–581, doi:10.1175/2009JCLI2662.1.

——, D. B. Chelton, and S. K. Esbensen, 2012: Covariability of surface wind and stress responses to sea surface temperature fronts. *J. Climate*, **25**, 5916–5942, doi:10.1175/JCLI-D-11-00230.1.

Pacanowski, R. C., 1987: Effect of equatorial currents on surface stress. *J. Phys. Oceanogr.*, **17**, 833–838, doi:10.1175/1520-0485(1987)017<0833:EOECOS>2.0.CO;2.

Park, K.-A., and P. C. Cornillon, 2002: Stability-induced modification of sea surface winds over Gulf Stream rings. *Geophys. Res. Lett.*, **29**, 2211, doi:10.1029/2001GL014236.

Renault, L., M. J. Molemaker, J. C. McWilliams, A. F. Shchepetkin, F. Lemarie, D. Chelton, S. Illig, and A. Hall, 2016: Modulation of wind work by oceanic current interaction with the atmosphere. *J. Phys. Oceanogr.*, **46**, 1685–1704, doi:10.1175/JPO-D-15-0232.1.

Saha, S., and Coauthors, 2010: The NCEP Climate Forecast System Reanalysis. *Bull. Amer. Meteor. Soc.*, **91**, 1015–1057, doi:10.1175/2010BAMS3001.1.

Seo, H., A. J. Miller, and J. R. Norris, 2016: Eddy–wind interaction in the California Current System: Dynamics and impacts. *J. Phys. Oceanogr.*, **46**, 439–459, doi:10.1175/JPO-D-15-0086.1.

Small, R. J., S. P. Xie, L. O'Neill, H. Seo, Q. Song, P. Cornillon, and S. Minobe, 2008: Air–sea interaction over ocean fronts and eddies. *Dyn. Atmos. Oceans*, **45**, 274–319, doi:10.1016/j.dynatmoce.2008.01.001.

Stern, M. E., 1975: *Ocean Circulation Physics*. Academic Press, 246 pp.

Sverdrup, H., 1947: Wind-driven currents in a baroclinic ocean: With application to the equatorial currents of the eastern Pacific. *Proc. Natl. Acad. Sci. USA*, **33**, 318–326, doi:10.1073/pnas.33.11.318.

Usui, N., H. Tsujino, Y. Fujii, and M. Kamachi, 2008a: Generation of a trigger meander for the 2004 Kuroshio large meander. *J. Geophys. Res.*, **113**, C01012, doi:10.1029/2007JC004266.

——, ——, H. Nakano, and F. Fujii, 2008b: Formation process of the Kuroshio large meander in 2004. *J. Geophys. Res.*, **113**, C08047, doi:10.1029/2007JC004675.

Winters, K. B., P. N. Lombard, J. J. Riley, and E. A. D'Asaro, 1995: Available potential energy and mixing in density stratified fluids. *J. Fluid Mech.*, **289**, 115–128, doi:10.1017/S002211209500125X.

Wunsch, C., and D. Roemmich, 1985: Is the North Atlantic in Sverdrup balance? *J. Phys. Oceanogr.*, **15**, 1876–1880, doi:10.1175/1520-0485(1985)015<1876:ITNAIS>2.0.CO;2.

Xie, S., 2004: Satellite observations of cool ocean–atmosphere interaction. *Bull. Amer. Meteor. Soc.*, **85**, 195–208, doi:10.1175/BAMS-85-2-195.

Xu, Y., and R. B. Scott, 2008: Subtleties in forcing eddy resolving ocean models with satellite wind data. *Ocean Modell.*, **20**, 240–251, doi:10.1016/j.ocemod.2007.09.003.

Yamagata, T., and S. Umatani, 1989: Geometry-forced coherent structures as a model of the Kuroshio large meander. *J. Phys. Oceanogr.*, **19**, 130–138, doi:10.1175/1520-0485(1989)019<0130:GFCSAA>2.0.CO;2.

Yasuda, I., J. Yoon, and N. Suginohara, 1985: Dynamics of the Kuroshio large meander: Barotropical model. *J. Oceanogr. Soc. Japan*, **41**, 259–273, doi:10.1007/BF02109275.

Yu, Z., and Coauthors, 2015: Seasonal cycle of volume transport through Kerama Gap revealed by a 20-year global Hybrid Coordinate Ocean Model reanalysis. *Ocean Modell.*, **96**, 203–213, doi:10.1016/j.ocemod.2015.10.012.

Zhai, X., and R. J. Greatbatch, 2007: Wind work in a model of the northwest Atlantic Ocean. *Geophys. Res. Lett.*, **34**, L04606, doi:10.1029/2006GL028907.

Zhu, X.-H., I.-S. Han, J.-H. Park, H. Ichikawa, K. Murakami, A. Kaneko, and A. Ostrovskii, 2003: The northeastward current southeast of Olinava Island observed during November 2000 to August 2001. *Geophys. Res. Lett.*, **30**, 1071, doi:10.1029/2002GL015867.

——, J.-H. Park, and I. Kaneko, 2005: The northeastward current southeast of the Ryukyu Islands in late fall of 2000 estimated by an inverse technique. *Geophys. Res. Lett.*, **32**, L05608, doi:10.1029/2004GL022135.